

Genome-scale clustered regularly interspaced short palindromic repeats screen identifies nucleotide metabolism as an actionable therapeutic vulnerability in diffuse large B-cell lymphoma

Nicholas Davies,^{1*} Tegan Francis,^{1*} Ceri Oldreive,¹ Maria Azam,¹ Jordan Wilson,¹ Philip J. Byrd,¹ Megan Burley,¹ Archana Sharma-Oates,² Peter Keane,¹ Sael Alatawi,^{1,3} Martin R. Higgs,¹ Zbigniew Rudzki,⁴ Maha Ibrahim,^{1,5} Tracey Perry,¹ Angelo Agathangelou,¹ Anne-Marie Hewitt,¹ Edward Smith,¹ Constanze Bonifer,¹ Mark O'Connor,⁶ Josep V. Forment,⁶ Paul G. Murray,⁷ Eanna Fennell,⁷ Gemma Kelly,⁸ Catherine Chang,⁸ Grant S. Stewart,¹ Tatjana Stankovic,¹ Marwan Kwok^{1,9} and Alexander Malcolm Taylor¹

¹Institute of Cancer and Genomic Sciences, University of Birmingham, Birmingham, UK;

²School of Biosciences, University of Birmingham, Birmingham, UK; ³Department of Medical Laboratory Technology, Faculty of Applied Medical Sciences, University of Tabuk, Tabuk, Saudi Arabia;

⁴Department of Histopathology, University Hospitals Birmingham NHS Foundation Trust, Birmingham, UK;

⁵South Egypt Cancer Institute, Assiut University, Assiut, Egypt; ⁶Bioscience Oncology R&D, AstraZeneca, Cambridge, UK; ⁷School of Medicine, Bernal Institute, Health Research Institute & LDCRC, University of Limerick, Limerick, Ireland;

⁸Blood Cells and Blood Cancer Division, The Walter and Eliza Hall Institute of Medical Research, Melbourne, Victoria, Australia and ⁹Center for Clinical Hematology, Queen Elizabeth Hospital Birmingham, Birmingham, UK

**ND and TF contributed equally as first authors.*

Correspondence: T. Stankovic
t.stankovic@bham.ac.uk

A.M. Taylor
a.m.r.taylor@bham.ac.uk


M. Kwok
m.kwok@bham.ac.uk

Received: October 4, 2023.

Accepted: May 24, 2024.

Early view: June 6, 2024.

<https://doi.org/10.3324/haematol.2023.284404>

Published under a CC BY license 

Supplementary Material

Supplementary Methods

Genotyping of *Atm*^{-/-}*nu*^{-/-} mice

Atm genotype was confirmed by PCR, utilizing primer pairs that recognize a consensus *Atm* sequence.¹

Cell lines

Human DLBCL cell lines were obtained from DSMZ (Braunschweig, Germany; BJAB, HT, OCI-LY1, OCI-LY3, RC-K8, SUDHL5, U2932, WILL-2), ATCC (Manassas, VA; Farage, HBL1) or ECACC (Porton Down, UK; KARPAS-422). Human Burkitt lymphoma cell lines were obtained from DSMZ (BJAB, DG75). Lymphoblastoid cell lines (LCL) were previously generated.² The CII-*ATM*/*GFP* CLL cell lines were previously generated from CII (obtained from Prof. A Rosen, Linköping University, Sweden).² All human cell lines were cultured in RPMI containing 10% FCS and 1% penicillin/streptomycin.

Murine *E μ -Myc* cell lines; modelling Burkitt lymphoma; were established from *E μ -Myc* transgenic lymphomas.³

Cytotoxicity assays

Cell lines were treated with MMF, AZD1775, pevonedistat (MLN4924; Selleckchem), MYC inhibitor (MYCi361; Selleckchem) and nucleosides (Sigma-Aldrich, Poole, UK) either alone or in combination. Cytotoxicity was determined by alamar blue uptake (Sigma-Aldrich), CellTiter-Glo (Promega, Southampton, UK), or propidium iodide (PI; Sigma-Aldrich) exclusion, and analyzed using a PHERAstar (BMG Labtech, Aylesbury, UK) or Enspire (PerkinElmer, Beaconsfield, UK) microplate reader or LSRFortessa™ X-20 Cell Analyzer (BD Biosciences, Oxford, UK). All experiments were performed at least in triplicate. Combination indices (CI) to identify synergism and 50% effective concentration (EC_{50}) were calculated using CalcuSyn (Biosoft, Cambridge, UK).

V(D)J recombination analysis

Sanger sequencing of *V(D)J* rearrangements was undertaken according to standard protocols.⁴ Analysis was carried out using the NCBI Ig Blast software.

FACS analysis

Cells were analyzed using a CyAn ADP FACS analyzer (Beckman Coulter, High Wycombe, UK) and Summit software (v4.3). Non-specific antibody binding was blocked by anti-mouse CD16/32 before staining with CD3, CD4-PE, CD8a-APC, CD5-APC, B220-E450, CD43-PE, IgM and IgD antibodies (eBiosciences, Altrincham, UK).

Cell cycle analysis was performed according to standard methods.⁵ Apoptosis was determined with an Annexin V (AxV) Apoptosis Detection kit (eBiosciences). γ H2AX expression was determined using γ H2AX-FITC antibody (Millipore, Watford, UK) and the Click-iT™ EdU Alexa Fluor™ 647 Flow Cytometry Assay Kit (ThermoFisher, Gloucester, UK). All analysed using the BD LSRFortessa™ X-20 and FlowJo v10.8.0.

Immunohistochemistry

Immunohistochemistry was performed using antibodies against B220 (BD Biosciences), CD20 (Life Technologies), CD21 (Abcam, Cambridge, UK), CD10 (Bioss, Boston, MA), CD3, IRF4 (Dako, Cambridge, UK; Abcam), BCL2 (Novus, Abingdon, UK), Ki67, PAX5 (BD Biosciences), and FOXP1 (AbD Serotec, Watford, UK).⁶

RNA-seq analysis

RNA was isolated from *Atm^{-/-}nu^{-/-}* lymphomas and *Atm^{+/+}nu^{-/-}* or *Atm^{+/-}nu^{-/-}* splenic B-cells using the RNeasy Micro Kit (Qiagen, Manchester, UK), quantified using Qubit, and quality assessed using TapeStation (Agilent, Manchester, UK). RNA-seq libraries generated using Neoprep mRNA kits (Illumina, Cambridge, UK) were sequenced on the NextSeq 500 platform (Illumina). For comparison, RNA-seq data of human DLBCL from the Cancer Genome Characterization Initiative (CGCI) study was downloaded from dbGap (<http://www.ncbi.nlm.nih.gov/gap>; accession phs000532)⁷ and the European Genome-Phenome Archive (EGAS00001002606).¹⁵ RNA-seq data for the control germinal center (GC) B-cell samples were obtained from the Gene Expression Omnibus (GEO; <http://www.ncbi.nlm.nih.gov/geo/>; accession GSE45982).⁸

Murine and human transcriptome data were aligned to GRCm38.p5 and hg19 respectively using Rsubread aligner, and assigned to individual genes using the Counts function (data available upon request).⁹ The edgeR package in R was used to normalize read counts between samples, convert to counts-per-million (CPM) reads for each gene and analyze differential expression between sample groups.¹⁰ Genes were considered to be differentially expressed if fold-change >2 and Benjamini-Hochberg adjusted P<0.05. Differential expression heatmaps were constructed using the gplots and ComplexHeatmap library in R. CPM values for each relevant gene were centered at zero, scaled separately and capped at +/- 3 before applying the Euclidean distance measure in conjunction with the Ward.D2 clustering algorithm. Kyoto Encyclopaedia of Genes and Genomes (KEGG) pathway analysis and Gene Set Enrichment Analysis (GSEA v3.0) were executed using clusterProfiler package in R.^{11,12}

Fluorescence in situ hybridization (FISH)

Metaphases (≤ 40) were analyzed using the ISIS software (Didcot, UK) and images captured using a Zeiss Axio imager (Birmingham, UK).^{13,14} The murine chromoprobe multiprobe octochrome system was used for M-FISH (Cytocell, Bicester, UK). Targeted-FISH probes were custom made from the following BAC: IgH alpha-5-ROX dUTP (RP23-455J10), IgH V1 5-Fluorescein dUTP (RP23-303N6) and c-Myc 5-ROX dUTP (RP23-307D14) (Empire Genomics, Buffalo, NY). Circos plots of chromosomal translocations were created using the Rcircos library in R.¹⁵

Western Blotting

Western blotting was performed using ATM (Sigma-Aldrich; Abcam), phospho (p)-ATM (Millipore), NBS1, p-NBS1 (Abcam), SMC1 (Bethyl, Montgomery, Texas, USA), MYC, RRM2, ATR, CHK1 (Santa Cruz, Wembley, UK), p-CHK1 (Cell Signaling, Leiden, Netherlands) VINCULIN or ACTIN (Sigma-Aldrich) primary antibodies and HRP-conjugated anti-rabbit or anti-mouse secondary antibodies (Dako). Immunoreactive bands were visualized using ECL solution and X-Ray film (GE Healthcare Life Sciences, Amersham, UK).⁴

Immunocytochemistry

Cell death was evaluated using 4',6-diamidino-2-phenylindole (DAPI; Sigma-Aldrich) counterstaining, goat anti-Lamin B (Atlas Antibodies, Stockholm, Sweden) and rabbit anti-p-

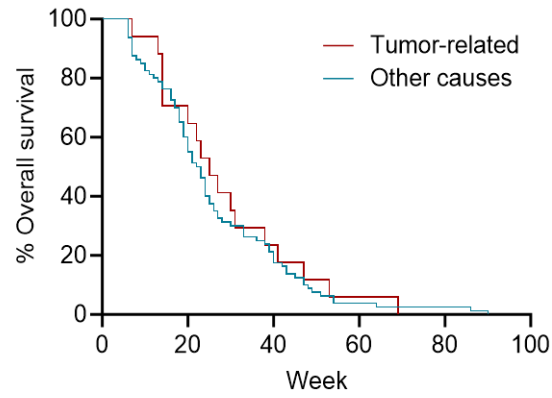
Histone H3 serine-10 (Cell Signaling) primary antibodies and anti-mouse (Alexa Fluor™ 594) and anti-rabbit (Alexa Fluor™ 488; Life Technologies) secondary antibodies² At least 100 cells were analyzed using a Nikon Eclipse E600 (Surbiton, Surrey).

DNA Fiber analysis

DNA fiber analysis was performed according to established protocols using idodeoxyuridine (IdU; Sigma-Aldrich), chlorodeoxyuridine (cldU; Sigma-Aldrich), rat- and mouse-bromodeoxyuridine (BrdU) antibodies (Abcam; BD Biosciences).¹⁶ DNA fibers were analyzed using ImageJ.

Supplementary Figures

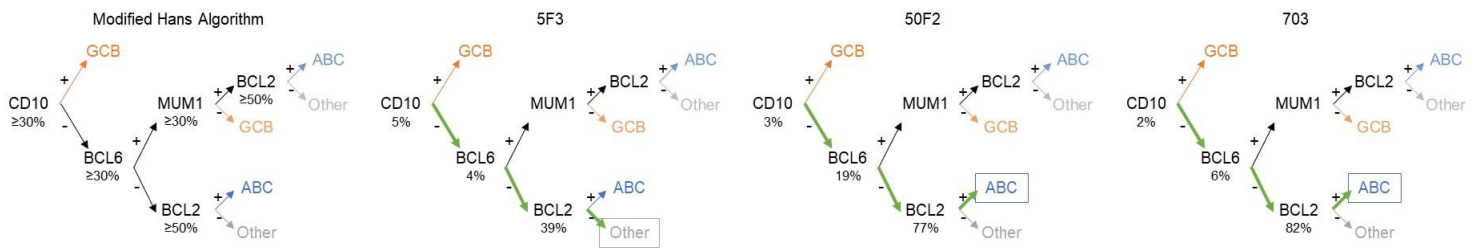
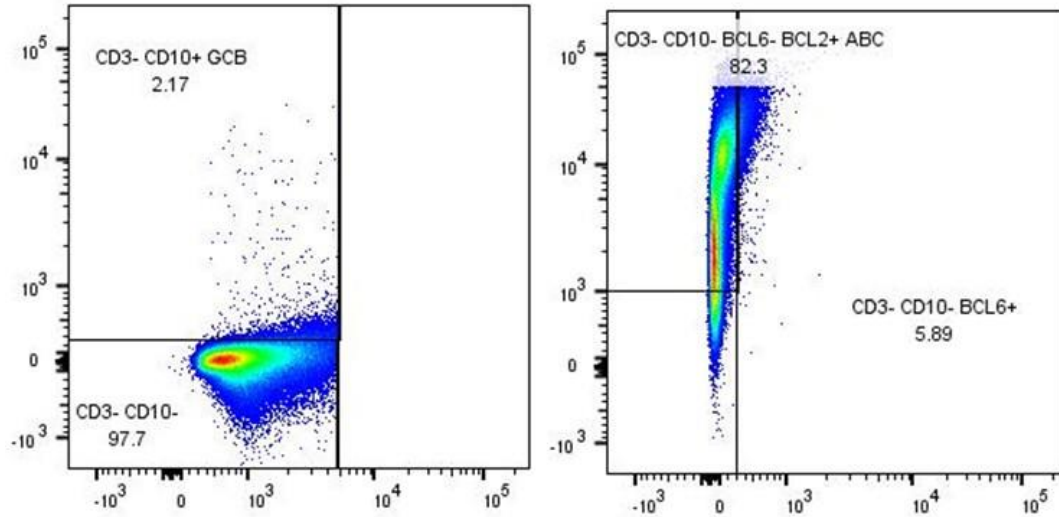
Figure S1. *Atm*^{-/-}*nu*^{-/-} mice that develop lymphoma have prolonged overall survival irrespective of the cause of death



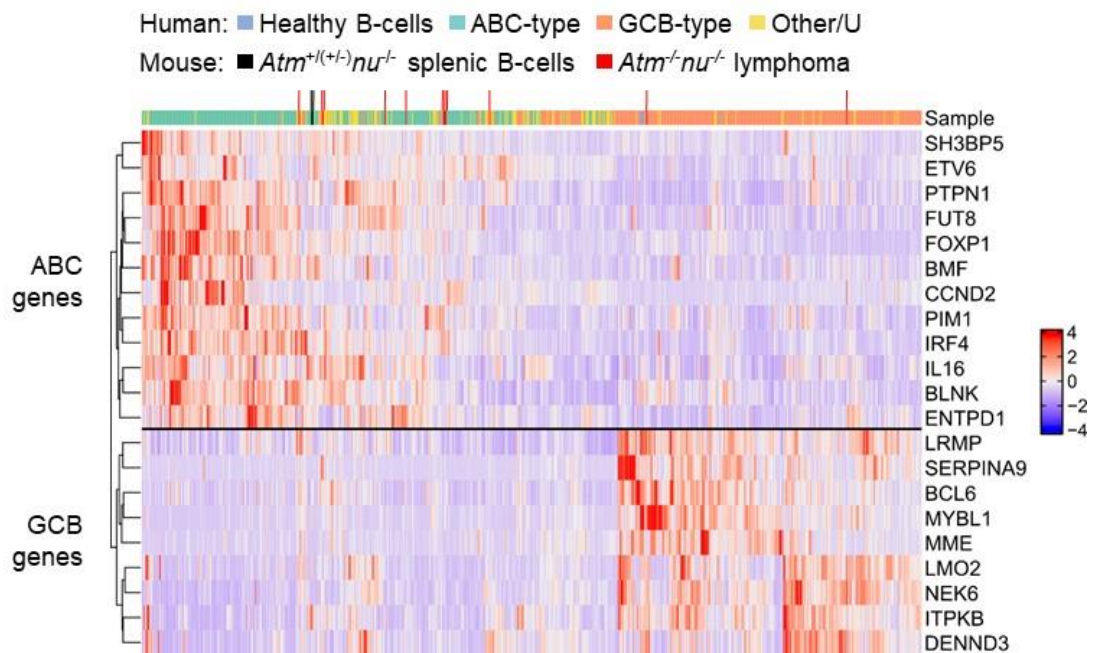
Kaplan-Meier curves displaying equivalent overall survival of *Atm*^{-/-}*nu*^{-/-} mice that have died due to lymphoma or other causes including infection ($P \leq 0.05$).

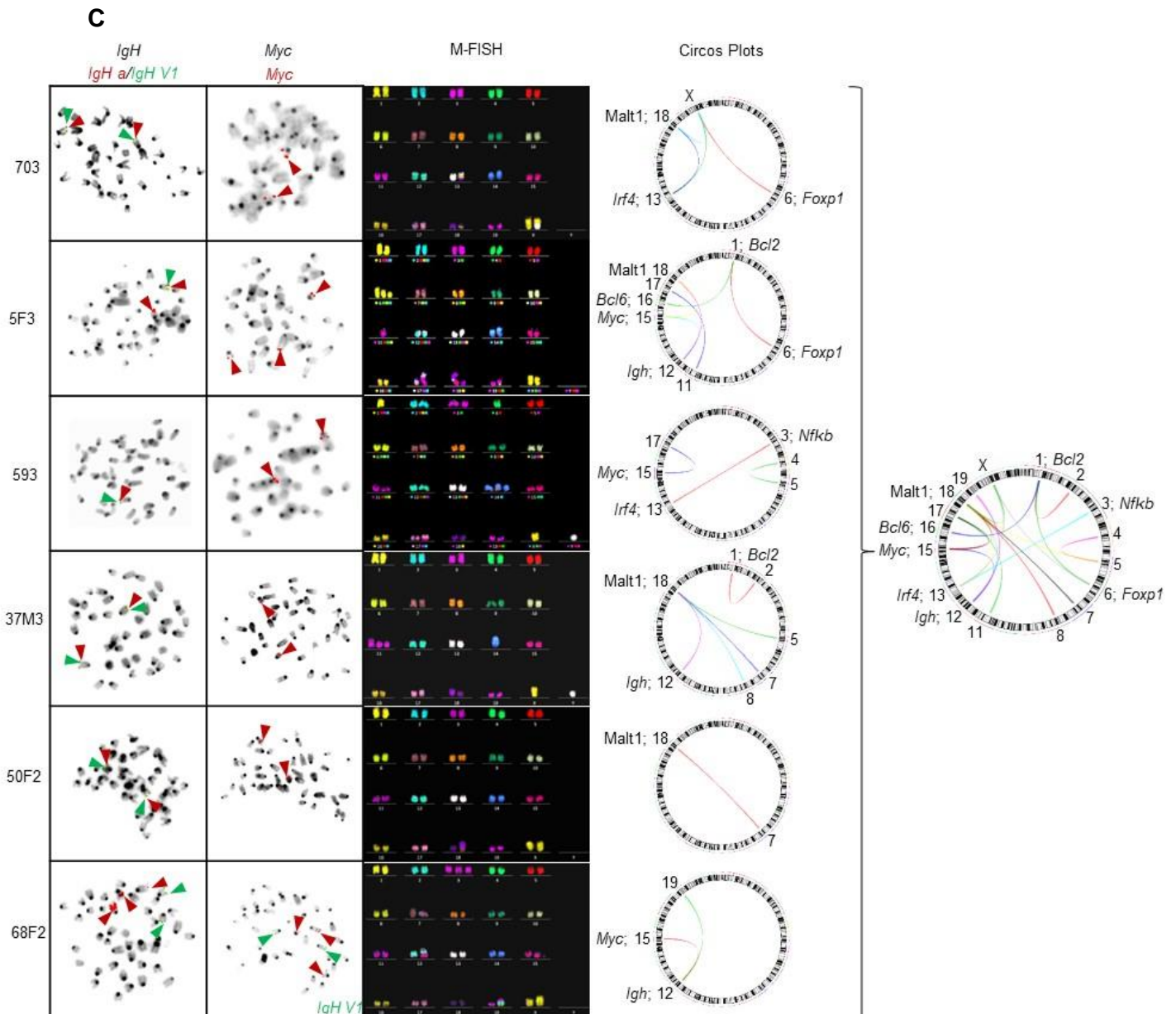
Figure S2. *Atm*^{-/-}*nu*^{-/-} mice develop B-cell lymphomas with complex karyotype that closely model human activated B-cell-like (ABC) and germinal center B-cell-like (GCB) diffuse large B-cell lymphoma (DLBCL)

A



B



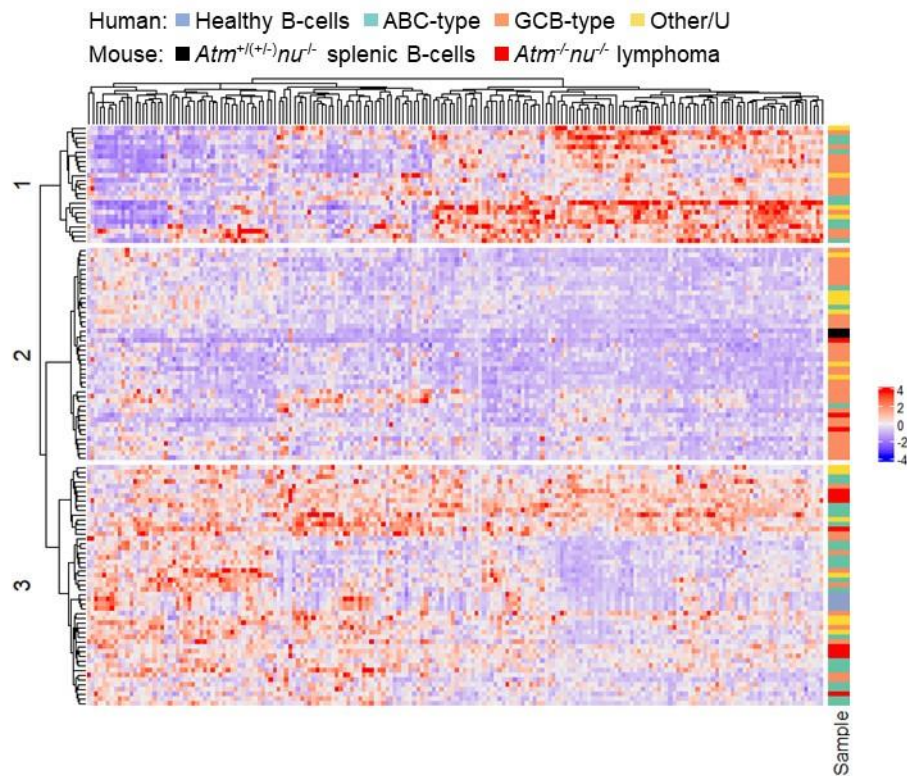


Characterization of the tumors derived from the *Atm^{-/-}nu^{-/-}* murine model. (A) Identification of cellular phenotype by FACS analysis of three cell lines established from *Atm^{-/-}nu^{-/-}* lymphomas (5F3, 50F2 and 703). Top: Representative FACS plots (703). Bottom: Cells comprising the murine DLBCL cell lines were classified as ABC (blue), GCB (orange) or other (grey) by sequential gating of subpopulations according to the Hans algorithm (<https://www.leukaemia.org.nz/content/uploads/2019/11/DLBCL-LNZ-Protocol-2019.pdf>) modified with the addition of BCL2 to differentiate non-GCB into ABC (BCL2⁺) and other (BCL2⁻) subtypes. The minimum percentage of cells expressing the marker to be considered positive for by immunohistochemistry is shown in the left hand diagram. Corresponding FACS analysis indicates that 50F2 and 703 cell lines are ABC DLBCL and 5F3 is other DLBCL. The outcome was confirmed upon replacement of MUM1 with FOXP1. (B) Comparison of

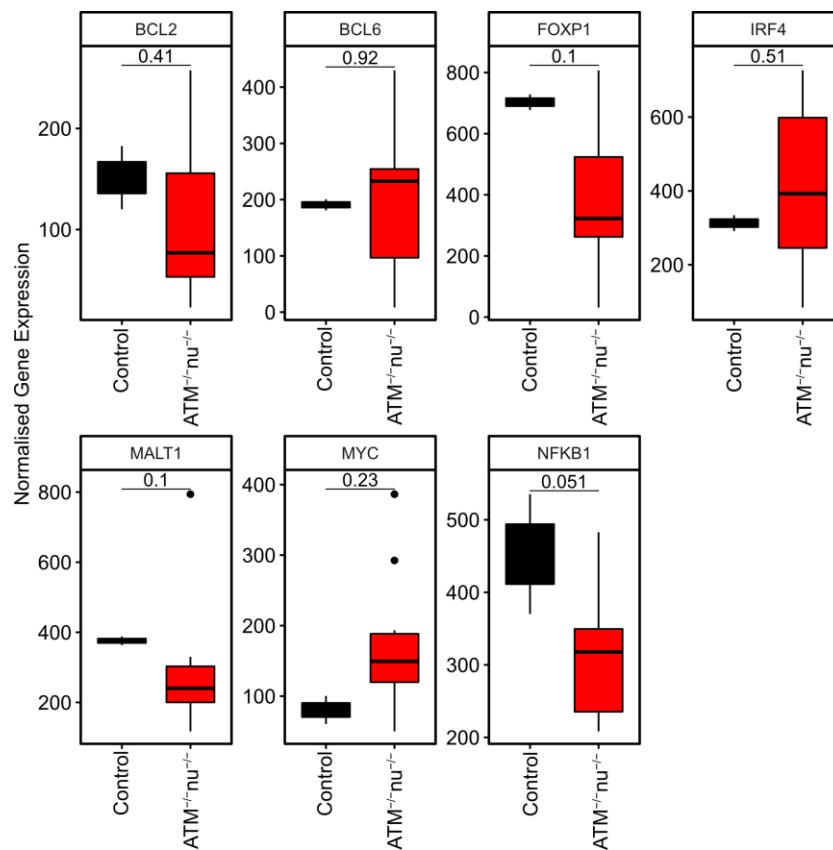
ribonucleic acid (RNA)-seq data of *Atm*^{-/-}*nu*^{-/-} lymphomas (n=11) and control splenic B-cells from *Atm*^{+/+}*nu*^{-/-} and *Atm*^{+/-}*nu*^{-/-} mice (n=2) against published RNA-seq datasets of human ABC DLBCL and healthy control germinal center (GC) B-cells^{7,8} suggests that the majority of *Atm*^{-/-}*nu*^{-/-} lymphomas cluster with human ABC DLBCL.¹⁷ (C) Specific translocations involving *IgH* and *MYC*, that are known drivers of *MYC* overexpression in human DLBCL, were specifically probed for by targeted-FISH whilst multiple cytogenetic alterations were detected by M-FISH in six representative *Atm*^{-/-}*nu*^{-/-} DLBCL. A normal metaphase spread should depict two copies of each targeted gene, with co-localization of the two *IgH* probes, as indicated by the arrows (703, 37M3, 50F2; *IgHa*, red; *IgHVi*, green; *Myc*, red). Differing copy numbers indicate gains and losses of the relevant gene (5F3, 593, 68F2). Translocations of the *IgH* locus were evidenced by non-co-localized staining of the *IgHa* and *IgHVi* probes, upon evidence of which, spreads were assessed for co-localization of *Myc* and *IgHVi* probes to identify whether *IgH-Myc* fusion had occurred (68F2). Whilst there was no evidence that *Atm*^{-/-}*nu*^{-/-} DLBCL harbored the human DLBCL *IgH-MYC* fusion, other abnormalities were detected: *Myc* gain (5F3, 68F2), *IgH* loss (5F3, 593), *IgH* translocation (68F2). The Circos plots depict the chromosomal interactions derived from identified aberrations for individual tumors and all 6 representative *Atm*^{-/-}*nu*^{-/-} B-cell lymphoma combined. Chromosomes are indicated by the numerals and annotated with lymphoma relevant genes localized in the regions affected by chromosomal alterations. No common translocation was observed.

Figure S3. *Myc* and *Myc* target gene expression is upregulated in *Atm*^{-/-}*nu*^{-/-} lymphomas

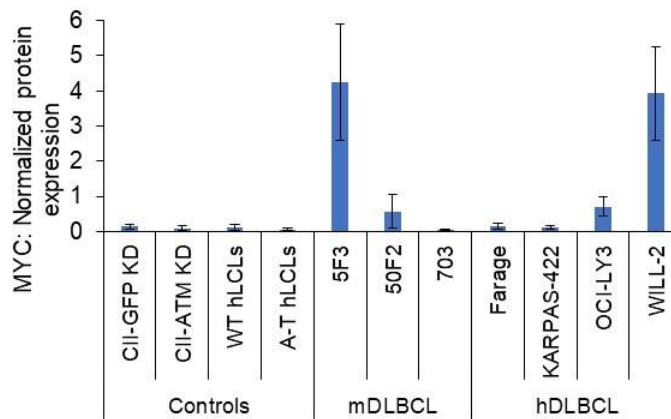
A



B

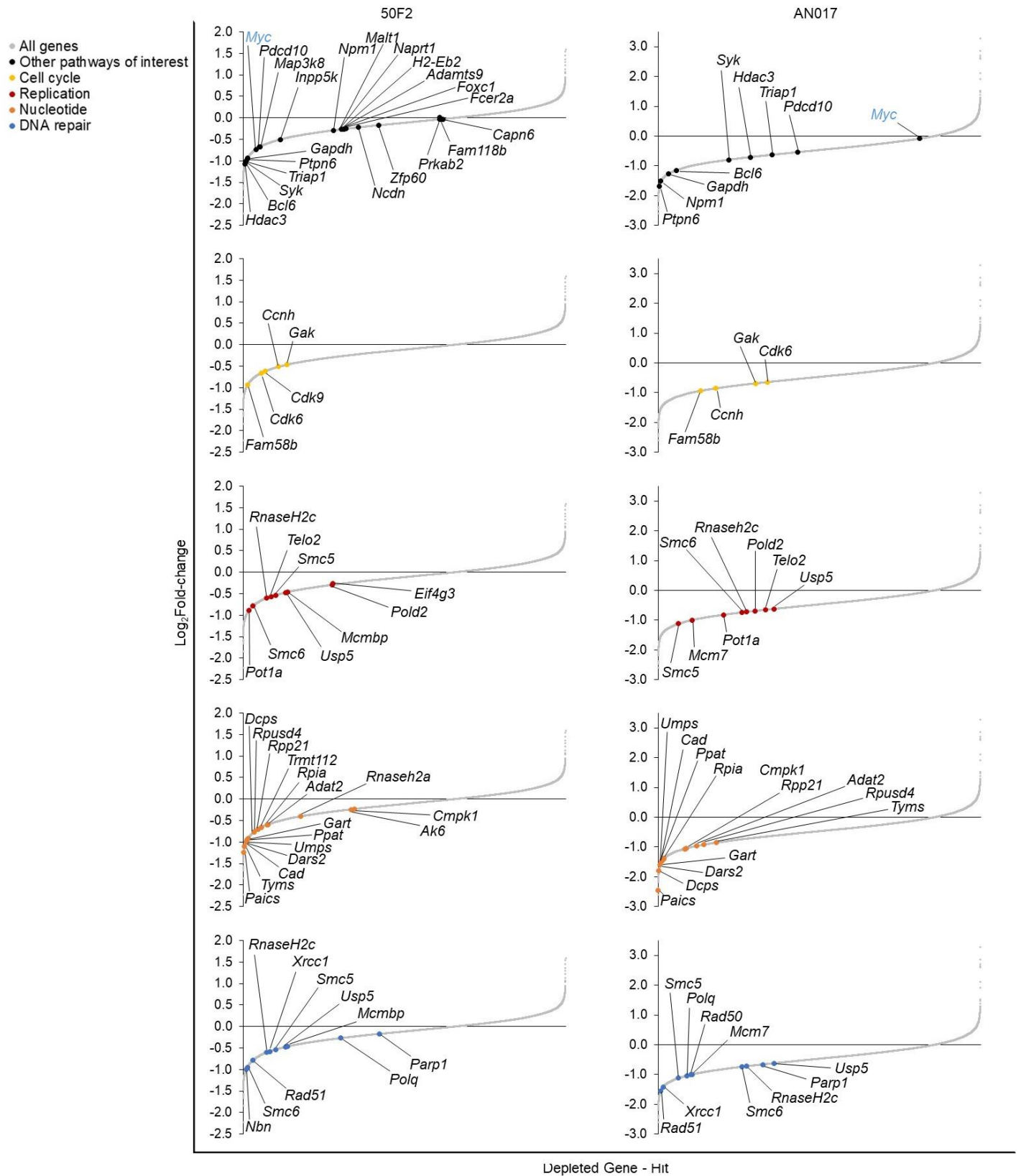


C



(A) Alignment of the transcriptional profiles of *Atm*^{-/-}*nu*^{-/-} lymphomas (n=12) and control splenic B-cells from *Atm*^{+/+}*nu*^{-/-} and *Atm*^{+/-}*nu*^{-/-} mice (n=2), human ABC DLBCL⁷ (n=32), GCB DLBCL⁷ (n=54), other/unknown (U) DLBCL (n=18) and healthy control GC B-cells⁸ (n=4) according to the expression of MYC target genes.¹⁸ This reveals that a high proportion of *Atm*^{-/-}*nu*^{-/-} DLBCL (red) align with a high (subset 3) MYC target gene-expressing group, whereas the *Atm*^{+/+}*nu*^{-/-} and *Atm*^{+/-}*nu*^{-/-} controls (black) align with the low (subset 2) MYC target gene-expressing group. (B) Compared to controls, RNA-seq analysis of *Atm*^{-/-}*nu*^{-/-} lymphomas (n=11) suggests differential upregulation of MYC but not other lymphoma relevant genes. (C) In comparison to human ATM WT and deficient tumor (CLL CII-cell line) and non-tumor (three healthy and A-T patient-derived LCL) controls, MYC protein expression is upregulated in two cell lines established from *Atm*^{-/-}*nu*^{-/-} lymphomas (5F3 and 50F2) and some human DLBCL cell lines (OCI-LY3 and WILL-2). Band intensities quantified using Image J were normalized to VINCULIN from ≥3 western blots and presented as mean ± SEM.

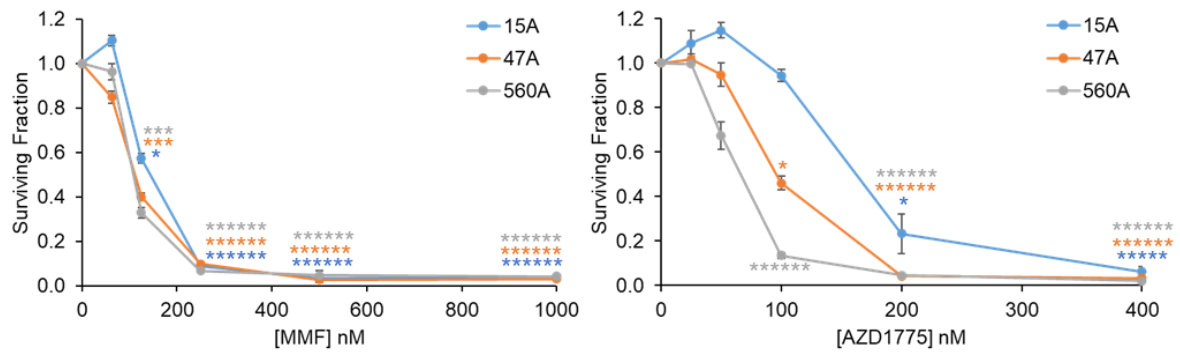
Figure S4. Cellular dependency pathways of *Atm^{-/-}nu^{-/-}* lymphomas identified by a genome-wide CRISPR/Cas9 screen



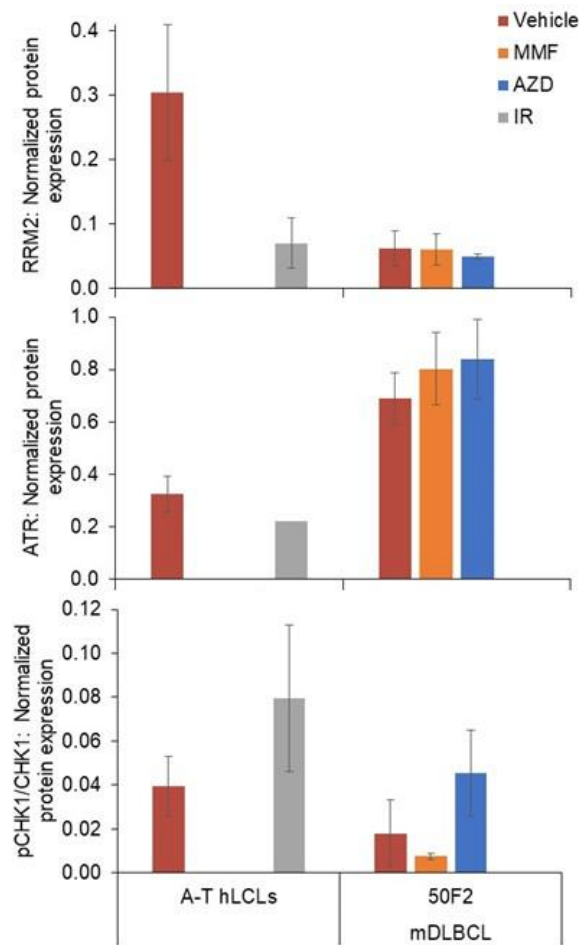
Identification of potential therapeutic targets for *Atm*^{-/-}*nu*^{-/-} lymphomas by genome-scale CRISPR/Cas9-mediated loss-of-function screen of two cell lines established from *Atm*^{-/-}*nu*^{-/-} lymphomas (50F2 and AN017) with an FDR <0.05. Constituent genes of each of the most significantly affected biological processes identified by RNA-seq, were depleted in both lymphoma cell lines and present potential therapeutic targets.

Figure S5. Nucleotide depletion induces cytotoxicity in $E\mu$ -Myc lymphoma and replication stress in MYC-dependent $Atm^{-/-}nu^{-/-}$ lymphomas

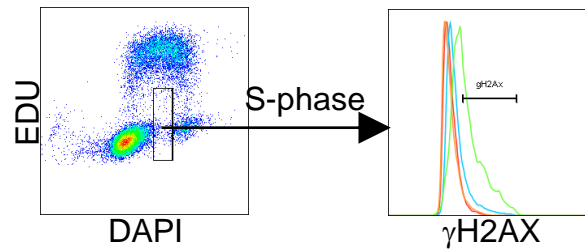
A



B

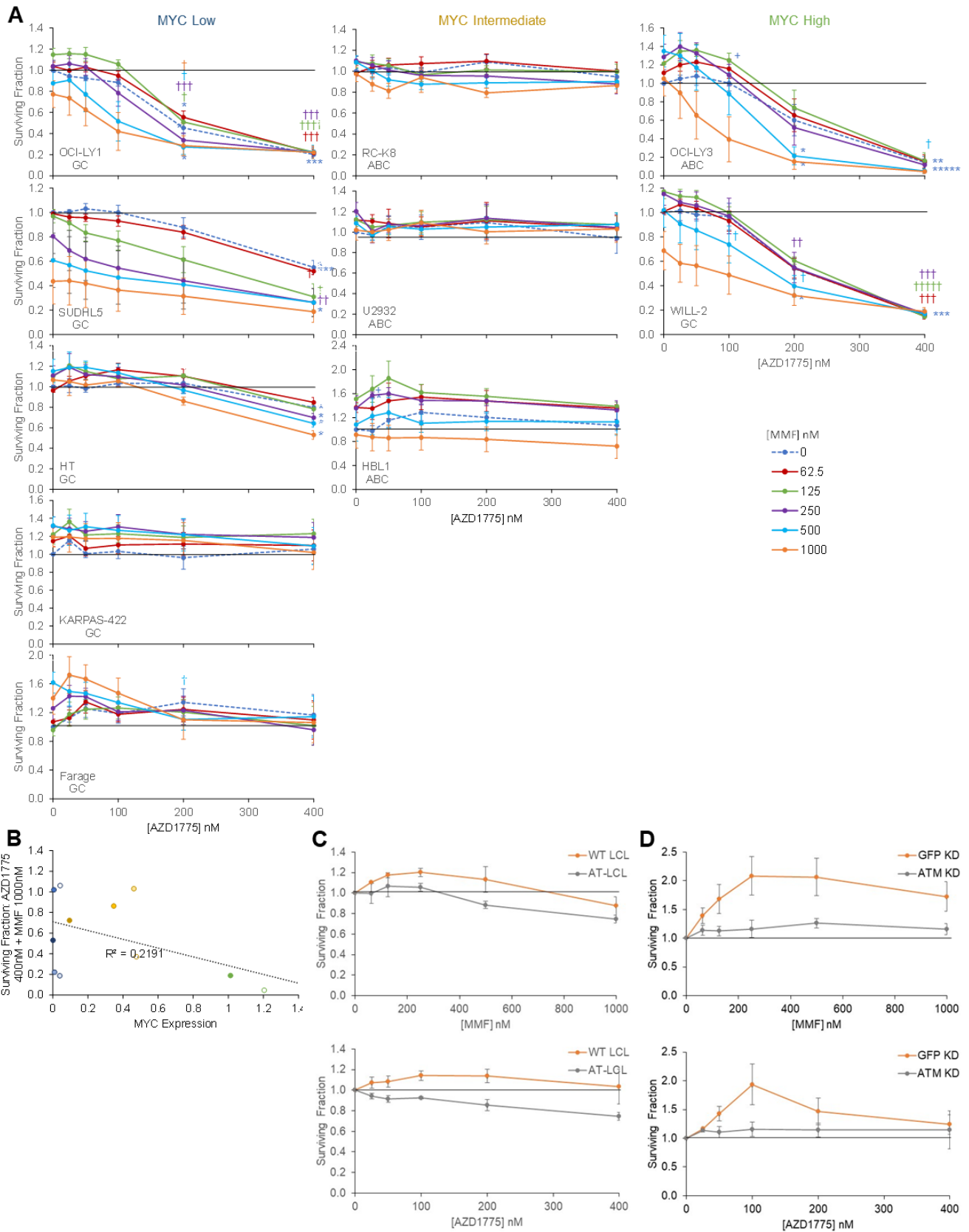


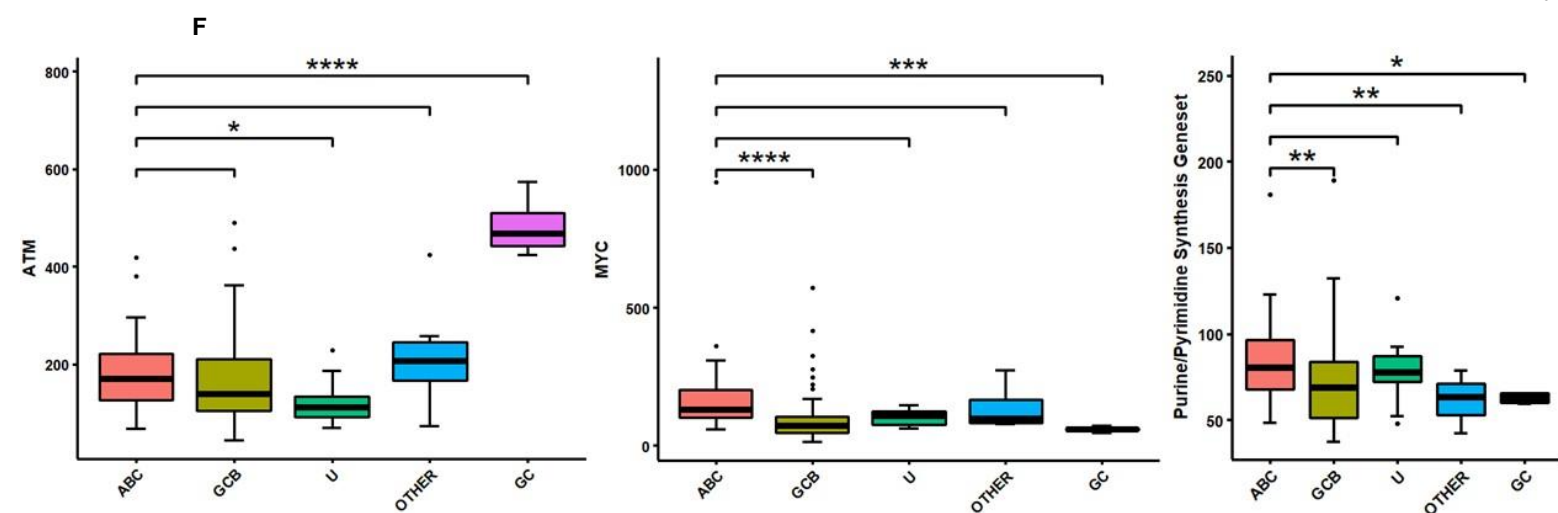
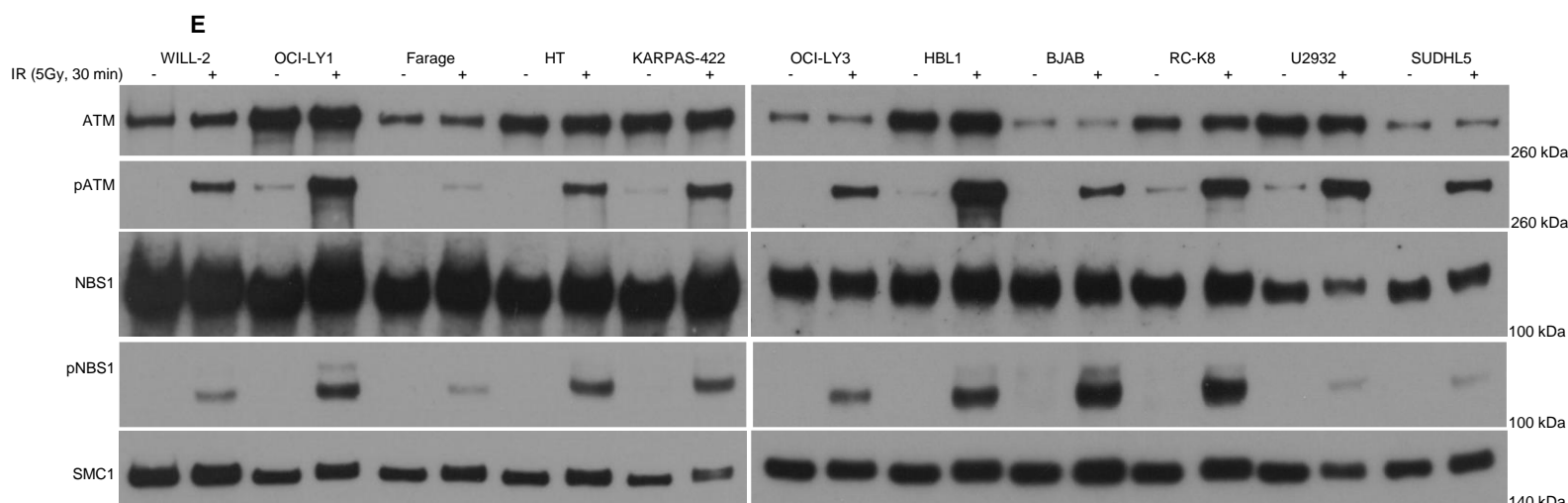
C



(A) Exposure (72h) of 3 *Atm* wild-type, *Eμ-Myc*-driven lymphoma cell lines to inhibitors of nucleotide synthesis (MMF or AZD1775; n=3) indicates sensitivity to both treatments as measured by Annexin V FACS analysis. Data presented as mean \pm SEM. Statistical significance versus untreated controls (*), was ascertained by repeat-measures matched multi-comparison one-way ANOVA with Tukey post-hoc test and denoted by: * $P \leq 0.05$, ** $P \leq 0.01$, *** $P \leq 0.005$, **** $P \leq 0.001$, ***** $P \leq 0.0005$, ***** $P \leq 0.0005$. (B) In comparison to human ATM-deficient non-tumor (three A-T patient-derived LCL) controls, basal RRM2 protein expression and a replicative stress indicator (phosphorylated CHK1 to total CHK1 protein ratio) are lower in a representative cell line established from an *Atm*^{-/-}*nu*^{-/-} lymphoma (50F2) whilst ATR is elevated. IR-induced (6Gy, 30min) replication stress in the A-T patient-derived LCL resulted in reduced RRM2 expression and concurrent elevated CHK1 phosphorylation which was replicated upon AZD1775 (500nM) but not MMF (250nM) treatment (72h) of an *Atm*^{-/-}*nu*^{-/-} lymphoma (50F2). Band intensities quantified using Image J were normalized to VINCULIN from ≥ 3 western blots and presented as mean \pm SEM. (C) The proportion of γ H2AX⁺ cells in non-replicating (inactive, quiescent) S-phase was determined by flow cytometry. Cell cycle stage was identified by DAPI staining and replicating cells by EDU. The dot plot illustrates the gating strategy employed to select non-replicating (EDU⁻) cells residing in S-phase in a representative vehicle-treated sample. The γ H2AX expression of EDU⁻ S-phase cells treated with vehicle (red), MMF (orange), AZD1775 (blue) or MMF + AZD1775 combined (green) cells on the right clearly demonstrates the accumulation of γ H2AX in non-replicating S-phase cells (EDU⁻ γ H2AX⁺) following combination treatment.

Figure S6. Elevated MYC expression sensitizes human DLBCL cells to nucleotide depletion

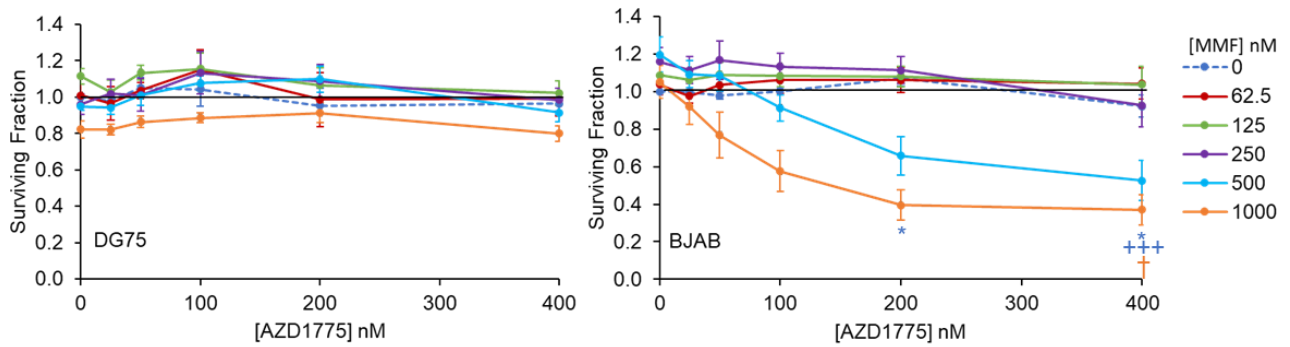




(A,B) Exposure (72h) of 11 human DLBCL cell lines with varying degrees of MYC expression to inhibitors of nucleotide synthesis (MMF or AZD1775; n=5) indicated a trend between MYC expression and increased cytotoxicity as measured by CellTitre-Glo for WEE1 inhibition (AZD1775). (C,D,E) Sensitivity to nucleotide synthesis inhibition is ATM-independent as evidenced by lack of differential sensitivity in (C) LCL cells derived from three healthy volunteers (WT LCL) versus three A-T patients (AT LCL) and (D) shRNA-ATM-KD CII cells (CLL tumor cell lines) and also (A,E) non-responsiveness of the sole cell line exhibiting loss of functional ATM (Farage); assessed by lack of multiple parameters of functional activity following irradiation (IR, 5 Gy, 30 min) of the cell lines. Samples were run on two separate gels. (F) Comparison of human DLBCL subsets and germinal centers by data-mining published human DLBCL RNA-seq datasets of human ABC DLBCL⁷ (n=32), GCB DLBCL⁷ (n=54), U DLBCL (n=10), Other DLBCL (n=8) and healthy control GC B-cells⁸ (n=4). In comparison to GC B-cells, patient ABC DLBCL expresses significantly reduced *ATM* whilst expression of both *MYC* and a purine/pyrimidine biosynthesis gene-set is higher in ABC-DLBCL than GC B-cells and GCB DLBCL. ABC, activated B-cell-like; GCB, germinal center

B-cell-like; U, unknown; Other, other; GC, germinal center B-cells. Statistical significance versus (A) untreated controls (*), AZD1775 (+) or MMF (†) concentration as denoted by symbol color, (C,D) untreated controls (*) or WT or GFP KD (+) as denoted by color, was ascertained by repeat-measures matched multi-comparison two-way ANOVA with Tukey post-hoc test and denoted by: * $P \leq 0.05$, ** $P \leq 0.01$, *** $P \leq 0.005$, **** $P \leq 0.001$, ***** $P \leq 0.0005$.

Figure S7. Human Burkitt lymphoma cells exhibiting high MYC expression are sensitive to nucleotide depletion



Exposure (72h) of human Burkitt lymphoma cell lines to inhibitors of nucleotide synthesis (MMF or AZD1775; n=5) indicates sensitivity to combined AZD/MMF treatment in BJAB (high MYC) but not DG75 (low MYC) (Figure S6E).¹⁹ Statistical significance versus untreated controls (*), AZD1775 (+) or MMF (†) concentration as denoted by symbol color, was ascertained by repeat-measures matched multi-comparison two-way ANOVA with Tukey post-hoc test and denoted by: * $P \leq 0.05$, ** $P \leq 0.01$, *** $P \leq 0.005$, **** $P \leq 0.001$, ***** $P \leq 0.0005$.

References

1. Liao MJ, Yin C, Barlow C, Wynshaw-Boris A, van Dyke T. Atm is dispensable for p53 apoptosis and tumor suppression triggered by cell cycle dysfunction. *Mol Cell Biol.* 1999;19(4):3095-3102.
2. Weston VJ, Oldreive CE, Skowronska A, et al. The PARP inhibitor olaparib induces significant killing of ATM-deficient lymphoid tumor cells in vitro and in vivo. *Blood.* 2010;116(22):4578-4587.
3. Adams JM, Harris AW, Pinkert CA, et al. The c-myc oncogene driven by immunoglobulin enhancers induces lymphoid malignancy in transgenic mice. *Nature.* 1985;318(6046):533-538.
4. Stankovic T, Stewart GS, Fegan C, et al. Ataxia telangiectasia mutated-deficient B-cell chronic lymphocytic leukemia occurs in pregerminal center cells and results in defective damage response and unrepaired chromosome damage. *Blood.* 2002;99(1):300-309.
5. Young LA, O'Connor LO, de Renty C, et al. Differential Activity of ATR and WEE1 Inhibitors in a Highly Sensitive Subpopulation of DLBCL Linked to Replication Stress. *Cancer Res.* 2019;79(14):3762-3775.
6. Oldreive CE, Skowronska A, Davies NJ, et al. T-cell number and subtype influence the disease course of primary chronic lymphocytic leukaemia xenografts in alymphoid mice. *Dis Model Mech.* 2015;8(11):1401-1412.
7. Morin RD, Johnson NA, Severson TM, et al. Somatic mutations altering EZH2 (Tyr641) in follicular and diffuse large B-cell lymphomas of germinal-center origin. *Nat Genet.* 2010;42(2):181-185.
8. Beguelin W, Popovic R, Teater M, et al. EZH2 is required for germinal center formation and somatic EZH2 mutations promote lymphoid transformation. *Cancer Cell.* 2013;23(5):677-692.
9. Liao Y, Smyth GK, Shi W. The Subread aligner: fast, accurate and scalable read mapping by seed-and-vote. *Nucleic Acids Res.* 2013;41(10):e108.
10. Robinson MD, McCarthy DJ, Smyth GK. edgeR: a Bioconductor package for differential expression analysis of digital gene expression data. *Bioinformatics.* 2010;26(1):139-140.
11. Subramanian A, Tamayo P, Mootha VK, et al. Gene set enrichment analysis: a knowledge-based approach for interpreting genome-wide expression profiles. *Proc Natl Acad Sci U S A.* 2005;102(43):15545-15550.
12. Mootha VK, Lindgren CM, Eriksson KF, et al. PGC-1alpha-responsive genes involved in oxidative phosphorylation are coordinately downregulated in human diabetes. *Nat Genet.* 2003;34(3):267-273.

13. Davies NJ, Kwok M, Gould C, et al. Dynamic changes in clonal cytogenetic architecture during progression of chronic lymphocytic leukemia in patients and patient-derived murine xenografts. *Oncotarget*. 2017;8(27):44749-44760.
14. Jacobsson B, Bernell P, Arvidsson I, Hast R. Classical morphology, esterase cytochemistry, and interphase cytogenetics of peripheral blood and bone marrow smears. *J Histochem Cytochem*. 1996;44(11):1303-1309.
15. Zhang H, Meltzer P, Davis S. RCircos: an R package for Circos 2D track plots. *BMC Bioinformatics*. 2013;14:244.
16. Da Costa D, Agathangelou A, Perry T, et al. BET inhibition as a single or combined therapeutic approach in primary paediatric B-precursor acute lymphoblastic leukaemia. *Blood Cancer J*. 2013;3:e126.
17. Wright G, Tan B, Rosenwald A, Hurt EH, Wiestner A, Staudt LM. A gene expression-based method to diagnose clinically distinct subgroups of diffuse large B cell lymphoma. *Proc Natl Acad Sci U S A*. 2003;100(17):9991-9996.
18. Liberzon A, Birger C, Thorvaldsdottir H, Ghandi M, Mesirov JP, Tamayo P. The Molecular Signatures Database (MSigDB) hallmark gene set collection. *Cell Syst*. 2015;1(6):417-425.
19. Barnouin K, Fredersdorf S, Eddaoudi A, et al. Antiproliferative function of p27kip1 is frequently inhibited in highly malignant Burkitt's lymphoma cells. *Oncogene*. 1999;18(46):6388-6397.

Supplementary Tables

Table S1. Classification features of *Atm*^{-/-}*nu*^{-/-} tumors

Microsoft Excel Table S1

Note: DLBCL, NOS, diffuse large B-cell lymphoma, not otherwise specified; +, present; ND, not done; -, not present; NA, not amplified; ~, undetermined; M, mutated; UM, unmutated.

Table S2. Cytogenetic profiles of *Atm*^{-/-}*nu*^{-/-} diffuse large B-cell lymphoma, not otherwise specified (DLBCL, NOS) tumors

Tumor code	M-FISH	Number of analysed cells	Targeted FISH		
	Cytogenetic aberrations		<i>Myc</i> copy number	<i>IgH</i> translocation	<i>IgH</i> loss
703	36~41, XX, der(X)t(X;13)[11], der(13)t(13;18)[9], der(18)t(18;X)[8], +6[4], -X[8], -4[4], -3[3], -5[5], -13[3], -15[3], -16[4], -17[4], -18[4], -19[3], add(6)[4], der(X)t(X;6)[3]	36	2	No	No
5F3	39~40, XX, der(17)t(11;17)[19], -11[17], -16[15], add(6)[15], dup(14)[5], der(18)t(15;12;18)*[8], der(18)t(15;18)*[8], der(6)t(1;6), der(1)t(1;16)[3]	20	3	No	Monoallelic <i>IgH V1</i>
593	39~40, XY, der(17)t(15;17)[19], -Y[6], -11[3], dup(4)[6], add(4)[6], der(13)t(3;13)[7], der(5)t(5;4)[4]	20	2	No	<i>IgH</i>
37M3	30~40, XY, der(18)t(12;18)[6], der(18)t(8;18)[4], der(18)t(5;18)[3], der(18)t(7;18)[3], -12[5], dup(18)[4], add(1)[3], add(3)[3], add(5)[3], add(11)[3], t(1;2)[5]	40	2	No	No
50F2	30~41, XX, dup(18)der(18)t(7;18)[12], -19[5], -5[4], -7[4], -8[4], -9[4], -2[3], -12[3], -16[3]	20	2	No	No
68F2	40, XX (Normal)[4]/40~41, XX, der(12)t(12;15)[8], -19[5], +3[5], +12[5], der(19)t(12;19)[3]	12	3	Yes	No

Note: FISH, fluorescence in-situ hybridization; M-FISH, multicolor-FISH; [#], denotes the number of cells in which the abnormality was detected;

*, Due to technical limitations of M-FISH analysis these aberrations have been denoted separately but could potentially be the same.

Table S3. RNA-seq: Significantly differentially expressed genes

Microsoft Excel Table S3

Note: baseMean, mean of normalized counts of all samples; log2FoldChange, effect size estimate of the expression change between comparison and control groups; lfcSE, standard error of the log2FoldChange; stat, Wald-log test statistic; pvalue, raw p-value; padj, false discovery rate p-value; 1-593.bam; *Atm*^{-/-}*nu*^{-/-} lymphoma sample (593 replicate 1) bam files; plus.minus.bam, control *Atm*^{+/-}*nu*^{-/-} splenic B-cell bam file; plus.plus.bam, control *Atm*^{+/+}*nu*^{-/-} splenic B-cell bam file.

Table S4. RNA-seq Kyoto Encyclopaedia of Genes and Genomes (KEGG) pathway analysis: Upregulated gene expression pathways

Microsoft Excel Table S4

Note: ID, unique identifier for each KEGG object; GeneRatio, fraction of differentially expressed genes found in the gene set; BgRatio, fraction of differentially expressed genes annotated to a pathway; p.adjust, corrected p-value using false discovery rate methods; qvalue, p-value using multiple hypothesis test correction indicates the probability that a reaction module was identified by chance; geneID, EntrezGene ID; Count, number of genes enriched in a KEGG pathway; Log_pvalue, log₁₀ of the p-value; Log_qvalue, log₁₀ of the q-value; Log_padjust, log₁₀ of the p.adjust-value.

Table S5. RNA-seq Kyoto Encyclopaedia of Genes and Genomes (KEGG) pathway analysis: Downregulated gene expression pathways

Microsoft Excel Table S5

Note: ID, unique identifier for each KEGG object; GeneRatio, fraction of differentially expressed genes found in the gene set; BgRatio, fraction of differentially expressed genes

annotated to a pathway; p.adjust, corrected p-value using false discovery rate methods; qvalue, p-value using multiple hypothesis test correction indicates the probability that a reaction module was identified by chance; geneID, EntrezGene ID; Count, number of genes enriched in a KEGG pathway; Log_pvalue, \log_{10} of the p-value; Log_qvalue, \log_{10} of the q-value; Log_padjust, \log_{10} of the p.adjust-value.

Table S6. RNA-seq Gene Set Enrichment Analysis (GSEA): Upregulated hallmarks

Microsoft Excel Table S6

Note: pval, nominal p value, the statistical significance of the enrichment score that is of limited use in comparing gene sets; padj, false discovery rate p-value; ES, enrichment score for the gene set, the degree to which this gene set is overrepresented at the top or bottom of the ranked list of genes in the expression dataset; NES, normalized enrichment score for the gene set; nMoreExtreme, number of times a control gene set had a more extreme enrichment score value, used to calculate nominal p-value; Size, number of genes present in the expression dataset; leadingEdge, subset of genes that contribute most to the ES.

Table S7. Clustered regularly interspaced short palindromic repeats (CRISPR): Comparison of sgRNA target gene expression at Day 18 vs Day 0 in two A-T DLBCL derived cell-lines

Microsoft Excel Table S7

Note: Score, MAGeCK Robust Rank Aggregation (RRA) enrichment score indicates the essentiality of a gene to identify 'hits'; FDR, false discovery rate.

Table S8. Clustered regularly interspaced short palindromic repeats (CRISPR) KEGG pathway analysis: Depleted gene (Hit) expression pathways

Microsoft Excel Table S8

ID, unique identifier for each Kyoto Encyclopaedia of Genes and Genomes (KEGG) object;
Observed gene Count, number of identified depleted genes in the KEGG pathway;
Background gene Count, number of total genes in the KEGG pathway; FDR, false discovery
rate; geneID, EntrezGene ID.